Article

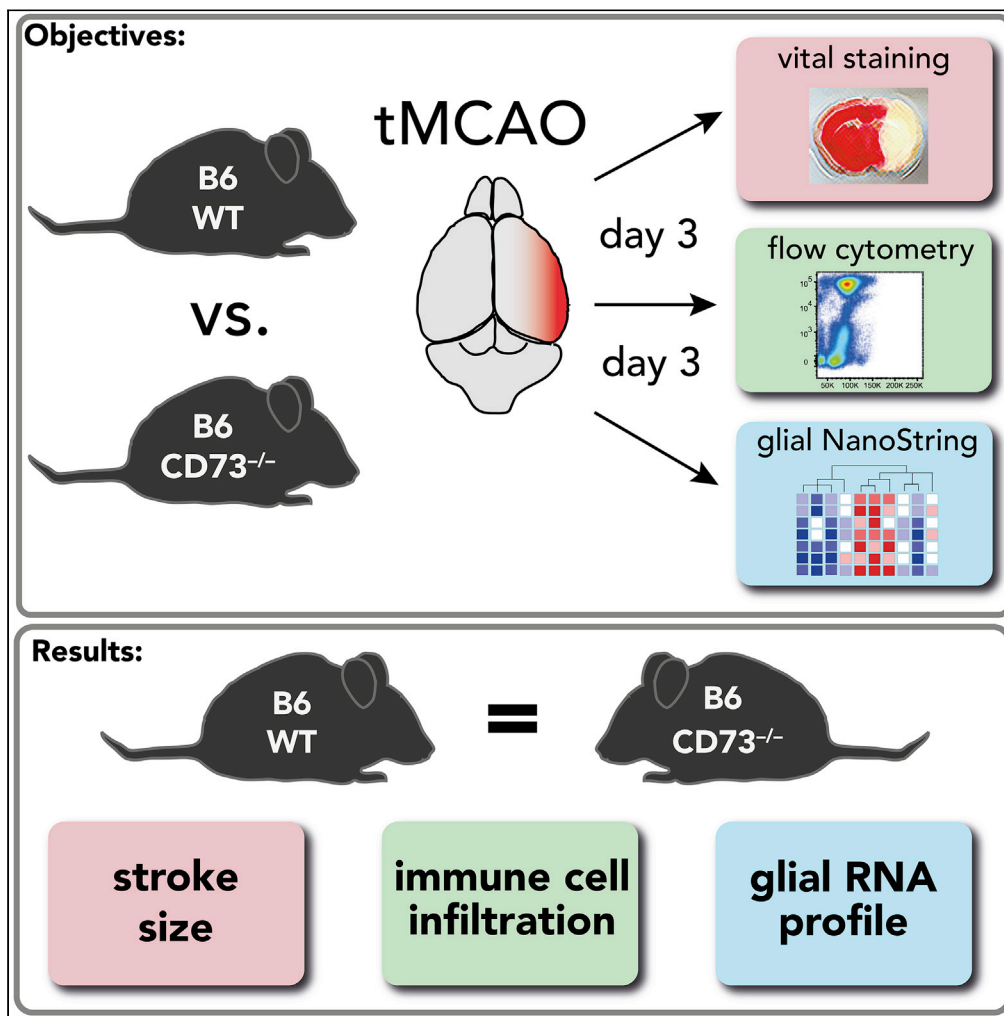# *Nt5e* deficiency does not affect post-stroke inflammation and lesion size in a murine ischemia/reperfusion stroke model

Ines Sophie Schädlich, Oliver Schnapauff, Lennart Pöls, Jürgen Schrader, Eva Tolosa, Björn Rissiek, Tim Magnus

i.schaedlich@uke.de (I.S.S.)
b.rissiek@uke.de (B.R.)

Highlights

Infarct volume on day 3 after tMCAO was comparable among CD73$^{-/-}$ and control mice

Brain leukocyte infiltration on day 3 after tMCAO was similar in CD73$^{-/-}$ and control mice

Glial RNA expression profile on day 3 after tMCAO was similar in CD73$^{-/-}$ and control mice

Article

Nt5e deficiency does not affect post-stroke inflammation and lesion size in a murine ischemia/reperfusion stroke model

Ines Sophie Schädlich,[1,*] Oliver Schnapauff,[1] Lennart Pöls,[1] Jürgen Schrader,[2] Eva Tolosa,[3] Björn Rissiek,[1,4,5,6,*] and Tim Magnus[1,4,6]

SUMMARY

Extracellular ATP released to the ischemic brain parenchyma is quickly metabolized by ectonucleotidases. Among them, the ecto-5′-nucleotidase CD73 encoded by *Nt5e* generates immunosuppressive adenosine. Genetic deletion of *Nt5e* led to increased infarct size in the murine photothrombotic stroke model. We aimed at validating this result using the transient middle cerebral artery occlusion (tMCAO) stroke model that represents pathophysiological aspects of penumbra and reperfusion. Three days after tMACO, we did not detect a difference in stroke size between CD73-deficient (CD73$^{-/-}$) and control mice. Consistent with this finding, CD73$^{-/-}$ and control mice showed comparable numbers and composition of brain-infiltrating leukocytes measured by flow cytometry. Using NanoString technology, we further demonstrated that CD73$^{-/-}$ and control mice do not differ regarding glia cell gene expression profiles. Our findings highlight the potential impact of stroke models on study outcome and the need for cross-validation of originally promising immunomodulatory candidates.

INTRODUCTION

Stroke ranks among the leading causes of death and disability worldwide (Krishnamurthi et al., 2020). Research over the last three decades revealed the substantial contribution of sterile inflammation to neuronal injury following ischemic stroke (Anrather and Iadecola, 2016; Planas, 2018; Iadecola et al., 2020). The excessive release of danger-/damage-associated molecular patterns (DAMP) such as adenosine triphosphate (ATP) from e.g. injured and dying neurons into the extracellular space initiate the inflammatory cascade in the ischemic brain parenchyma (Anrather and Iadecola, 2016; Petrovic-Djergovic et al., 2016). Extracellular pro-inflammatory ATP is degraded by ectonucleotidases: CD39 (ecto-nucleoside triphosphate diphosphohydrolase 1) metabolizes ATP to adenosine diphosphate (ADP) and adenosine monophosphate (AMP) and CD73 (ecto-5′-nucleotidase) dephosphorylates AMP to finally generate adenosine (ADO) (Colgan et al., 2006), which is neuroprotective (Burnstock, 2016) and anti-inflammatory (Antonioli et al., 2013). Since CD73 catalyzes the last step in the production of ADO, it has the potential to modulate the pro-inflammatory microenvironment after ischemic stroke by generating anti-inflammatory ADO. ADO can bind to four subtypes of adenosine receptors (AR), A_1, A_{2A}, A_{2B}, and A_3, which all belong to the superfamily of G-protein-coupled receptors and differ regarding their affinity for ADO and tissue distribution (Jacobson and Gao, 2006). For example, A_{2A} AR activation on immune cells has anti-inflammatory effects (Ohta and Sitkovsky, 2001; Ohta et al., 2009), ADO generation by CD73 and signaling through A_{2B} AR mediates cardioprotection by ischemic preconditioning (Eckle et al., 2007), and activation of both A_{2A} and A_{2B} ARs on peripheral vascular endothelial cells enhances barrier function and protects from inflammation- or hypoxia-induced development of edema (Aslam et al., 2021). Of note, hypoxia leads to CD73 up-regulation via hypoxia-inducible factor 1α (HIF1A) (Synnestvedt et al., 2002) further qualifying CD73 as an interesting target to study in ischemic stroke.

In mice, CD73 is expressed on all T cells, bone marrow neutrophils, peritoneal macrophages, and germinal center B cells (Immunological Genome Project). In the murine brain, CD73 constitutes the bulk of all AMP-hydrolyzing capacity within the CNS (Kulesskaya et al., 2013) and CD73 expression was immunohistochemically shown to be highest in basal ganglia (striatum and globus pallidus), but also present in the olfactory tubercle, the choroid plexus, and the meninges (Mills et al., 2008; Petrovic-Djergovic et al., 2012; Augusto

[1]Department of Neurology, University Medical Centre Hamburg-Eppendorf, Martinistraße 52, 20246 Hamburg-Eppendorf, Germany

[2]Department of Molecular Cardiology, Medical Faculty and University Hospital Düsseldorf, Heinrich-Heine-University Düsseldorf, Düsseldorf, Germany

[3]Institute of Immunology, University Medical Centre Hamburg-Eppendorf, Hamburg, Germany

[4]Senior authors

[5]Lead contact

[6]These authors contributed equally

*Correspondence:
i.schaedlich@uke.de (I.S.S.),
b.rissiek@uke.de (B.R.)

https://doi.org/10.1016/j.isci.2022.104470

et al., 2013; Kulesskaya et al., 2013). It has to be noted that, in contrast to human brain endothelial cells (Niemelä et al., 2008), CD73 could not be detected on mouse brain endothelial cells *in vivo* (Mills et al., 2008; Petrovic-Djergovic et al., 2012). Within the CNS, CD73 plays a versatile role ranging from locomotion (Kulesskaya et al., 2013), thermoregulation (Muzzi et al., 2013), neuronal activity, and cortical plasticity (Blundon et al., 2017; Badimon et al., 2020) to neuroinflammation in the context of experimental autoimmune encephalomyelitis (Mills et al., 2008), stroke (Petrovic-Djergovic et al., 2012) or neurodegenerative disorders like Parkinson's disease (Meng et al., 2019).

After photothrombotic stroke, mice deficient for CD73 exhibited larger infarcts and increased immune cell infiltration into the ischemic hemisphere than wild-type mice (Petrovic-Djergovic et al., 2012). However, the photothrombotic stroke model has three major translational disadvantages. First, it induces a pronounced vasogenic edema, which is not present to the same extent in human stroke, second, the irreversibly injured infarct core is not surrounded by ischemic tissue capable of surviving, the so-called tissue at risk or penumbra, and third, the vessel is occluded permanently not allowing reperfusion (Sommer, 2017). Reperfusion is of special interest as several publications highlight CD73-mediated protection in ischemic preconditioning and ischemia-reperfusion injury in peripheral organs like heart (Eckle et al., 2007), liver (Hart et al., 2008), or kidney (Sung et al., 2017).

Therefore, we aimed to re-evaluate the suggested protective role of CD73 in murine ischemic stroke using the transient intraluminal filament model better resembling the pathophysiological processes in human stroke. In addition to the analysis of stroke size in CD73$^{-/-}$ and control mice three days after transient middle cerebral artery occlusion, we investigated the effects of CD73 deficiency both on brain-infiltrating immune cells and resident glia cells as their interplay determines the extent of neuronal damage after ischemic stroke.

RESULTS

Genetic deletion of Nt5e does not affect ischemic lesion size in the tMCAO model

To determine whether CD73 influences stroke outcome in the setting of ischemia-reperfusion injury induced by the transient intraluminal filament model, we generated CD73$^{-/-}$ mice by cross-breeding CD73$^{fl/fl}$ mice with deleter mice that express the Cre recombinase in the germline (Schwenk et al., 1995) (Figure 1A). Absence of CD73 in CD73$^{-/-}$ mice was confirmed by flow cytometry of peritoneal macrophages, which expressed high levels of CD73 in CD73$^{fl/fl}$ control mice according to published expression data from wild-type mice (Immunological Genome Project) (Figure 1B). Cerebral CD73 deficiency in CD73$^{-/-}$ mice was further demonstrated by flow cytometry of oligodendrocytes, which are known to show the highest CD73 expression among brain-resident cells (Zamanian et al., 2012) (Figure 1B).

Next, we subjected CD73$^{-/-}$ and CD73$^{fl/fl}$ mice to 50 min of tMCAO. To rule out insufficient occlusion as a confounding variable with significant influence on infarct volume, regional cerebral blood flow (rCBF) was controlled by transcranial temporal laser Doppler after filament insertion. We did not detect a difference in ipsilateral rCBF (72.4 $\pm$ 23.4 a.u. versus 59.6 $\pm$ 25.5 a.u.) or contralateral rCBF (841.3 $\pm$ 63.6 a.u. versus 853.8 $\pm$ 50.7 a.u.) between CD73$^{-/-}$ and CD73$^{fl/fl}$ mice (Figure 1C). Laser Doppler measurements confirmed a drastic reduction (more than 90%) in blood flow in the left MCA territory compared to the contralateral side in both CD73$^{-/-}$ and CD73$^{fl/fl}$ mice (remaining blood flow 8.59 $\pm$ 2.61% compared with 6.95 $\pm$ 2.86%, respectively). Rectal body temperature of CD73$^{-/-}$ mice was significantly lower than that of CD73$^{fl/fl}$ mice at filament insertion (36.12 $\pm$ 0.44°C compared with 36.62 $\pm$ 0.28°C, respectively; p = 0.003) but converged during occlusion period and there was no significant difference detectable any more at the time of filament removal (36.05 $\pm$ 0.4°C compared with 36.4 $\pm$ 0.47°C, respectively; p = 0.0534) (Figure 1C). Initially lower body temperature might be explained by excessive AMP in CD73$^{-/-}$ mice mediating hypothermia via prolonged A$_1$ AR signaling in the hypothalamus (Muzzi et al., 2013). There was no difference in peripheral oxygen saturation between the two genotypes (Figure 1C).

Cerebral infarct volumes were analyzed three days after tMCAO in both CD73$^{-/-}$ and CD73$^{fl/fl}$ mice using vital staining with 2% (w/v) 2,3,5-triphenyl-2-hydroxy-tetrazolium chloride (TTC) (Figure S1). There was no significant difference in edema-corrected infarct volumes between CD73-deficient and control animals (66.6 $\pm$ 18.62 mm^3 compared with 73.96 $\pm$ 18.46 mm^3, respectively; p = 0.2984) (Figure 1D). The relative contribution of cerebral edema to uncorrected infarct volumes was identical in CD73$^{-/-}$ and CD73$^{fl/fl}$ mice (10.05 $\pm$ 5.98% compared with 10.58 $\pm$ 7.34%, respectively).
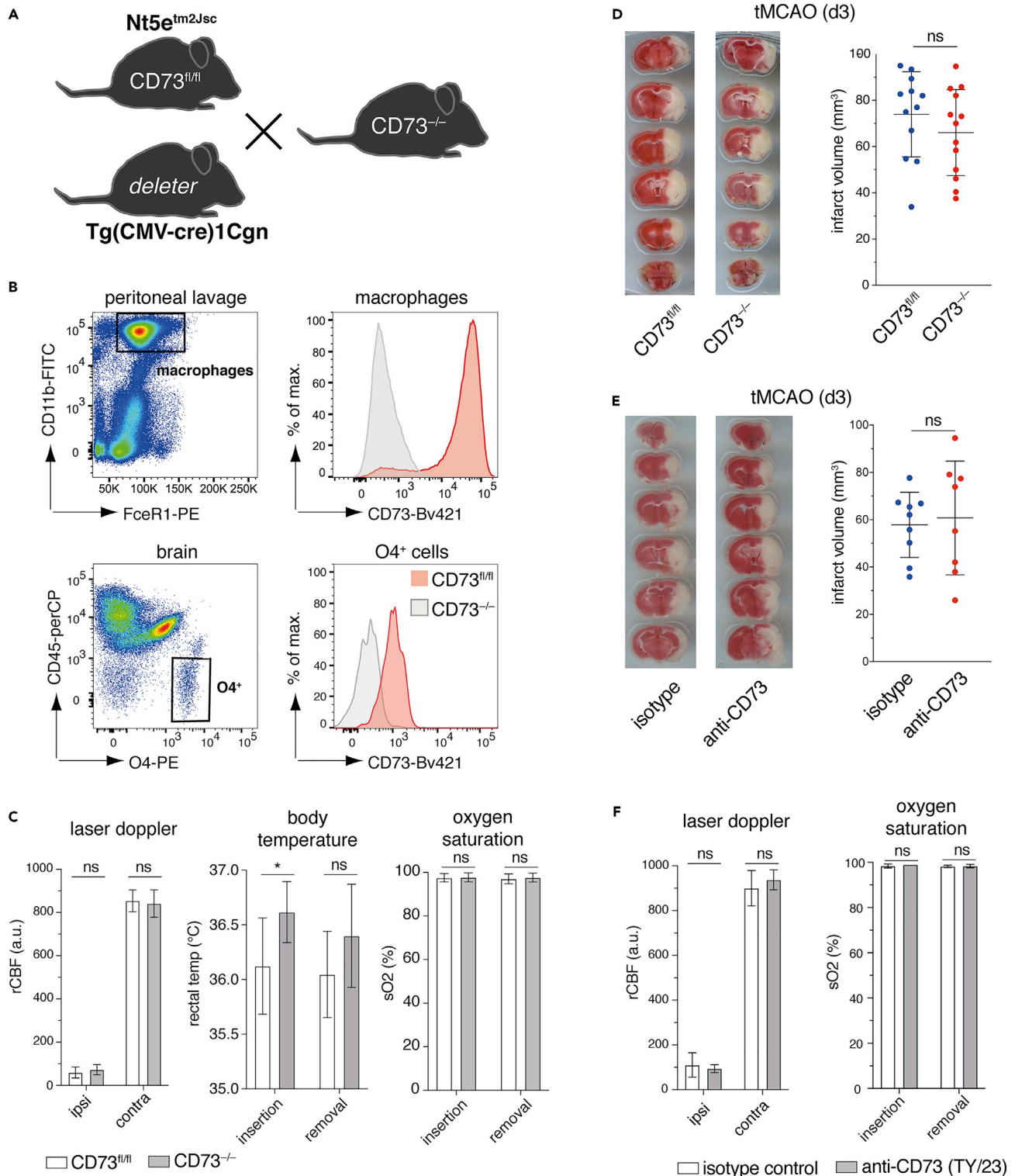
Figure 1. Effect of global CD73 deficiency on stroke outcome after tMCAO

(A) Generation of CD73$^{-/-}$ mice by crossing CD73$^{fl/fl}$(Nt5e^{tm2Jsc}) mice with a "deleter" cre-transgenic mouse strain (Tg(CMV-cre)1Cgn) mediating the deletion of loxP-flanked genes in all tissues including germ cells (Schwenk et al., 1995).

(B) Verification of *Nt5e* deletion in CD73$^{-/-}$ mice by comparing CD73 cell surface staining on CD73$^{-/-}$ and CD73$^{fl/fl}$ peritoneal macrophages (n = 3/group) and on CD73$^{-/-}$ and CD73$^{fl/fl}$ oligodendrocytes (n = 2/group).

Figure 1. Continued

(C) Physiological parameters of CD73$^{-/-}$ and CD73$^{fl/fl}$ mice: regional cerebral blood flow (rCBF) in the ipsilateral and contralateral MCA territory measured by laser Doppler (n = 8–12/group), rectal body temperature at filament insertion and removal (n = 12–13/group), peripheral oxygen saturation at the hind paw at filament insertion and removal (n = 12–13/group). Data are presented as mean ± SD, unpaired two-sided Student's t test, * p ≤ 0.05, ns = not significant.

(D) Representative TTC images and edema-corrected infarct volume measured by TTC staining of brain sections three days after tMCAO of CD73$^{-/-}$ and CD73$^{fl/fl}$ mice (n = 12–13/group). Data are presented as mean ± SD, unpaired two-sided Student's t test, ns = not significant.

(E) Representative TTC images and edema-corrected infarct volume measured by TTC staining of brain sections three days after tMCAO of anti-CD73 and isotype control treated C57BL/6J mice (n = 8–9/group). Data are presented as mean ± SD, unpaired two-sided Student's t test, ns = not significant.

(F) Physiological parameters of anti-CD73 and isotype control treated C57BL/6J mice: regional cerebral blood flow (rCBF) in the ipsilateral and contralateral MCA territory measured by laser Doppler (n = 5–8/group) and peripheral oxygen saturation at the hind paw at filament insertion and removal (n = 5–8/group). Data are presented as mean ± SD, unpaired two-sided Student's t test, ns = not significant.

To rule out compensatory changes during development as a consequence of germline deletion, we additionally performed acute blockade of CD73 in C57BL/6J wild-type mice by peripheral injection of an anti-CD73 antibody right before and 24 h after the induction of ischemic stroke by tMCAO. In line with the results obtained from transgenic mice, acute blockade of CD73 did not affect edema-corrected stroke volume on day three compared to isotype control treated animals (60.74 ± 24.01 mm^3 compared with 57.84 ± 13.79 mm^3, respectively; p = 0.7615) (Figures 1E and S1). Again, we did not detect a difference in ipsilateral or contralateral rCBF and peripheral oxygen saturation between the two experimental groups (Figure 1F).

Since hypoxia induces upregulation of CD73 on murine intestinal epithelial cells (Synnestvedt et al., 2002) and AR signaling modulates permeability of the blood–brain barrier (BBB) (Carman et al., 2011), we analyzed *Nt5e* expression on cortical microvessel cells from C57BL/6J wild-type mice after stroke by RT-qPCR. However, we did not detect any upregulation of *Nt5e* on cortical microvessels in the ischemic hemisphere compared to the contralateral hemisphere one day after tMCAO, whereas *Tnc* as a positive control with known upregulation on ischemic murine brain endothelial cells (Munji et al., 2019) showed a 6-fold upregulation compared to the contralateral hemisphere (Figure S2). Moreover, we investigated *Nt5e* expression and potential ischemia-induced upregulation on microglia but did not detect *Nt5e* expression in FACS isolated microglia neither under steady-state conditions nor one day post stroke in the ipsilateral and contralateral hemisphere (n = 4–5/group).

Genetic deletion of Nt5e does not affect infiltration of immune cells after tMCAO

Since immune cell recruitment to the ischemic hemisphere and subsequent sterile inflammation contribute decisively to tissue damage after cerebral ischemia and CD73 has been associated with leukocyte infiltration into the brain in other models of neuroinflammation, we next used flow cytometric analyses to investigate immune cell infiltration into the ipsilateral and contralateral hemisphere of CD73$^{-/-}$and CD73$^{fl/fl}$ mice three days after tMCAO. The timepoint of three days was chosen because it was previously identified as the peak of inflammation in the infarcted hemisphere (Gelderblom et al., 2009). After exclusion of debris, doublets, and dead cells, microglia were identified as CD45^{int}/CD11b$^+$ (Figure 2A). CD45^{hi}/CD11b$^+$ cells were subdivided into Ly6C^{int}/Ly6G$^+$ neutrophils and Ly6C^{hi}/Ly6G$^-$ monocytes/macrophages. Lymphocytes were gated as CD45^{hi}/CD11b$^-$ and further separated into CD4$^+$, CD8$^+$, and γδ T cells.

In accordance with stroke outcome, CD73$^{-/-}$ and CD73$^{fl/fl}$ mice had similar numbers of microglia, and of infiltrating neutrophils, Ly6C^{high} monocytes/macrophages, CD4$^+$ T cells, CD8$^+$ T cells, and γδ T cells in both the ipsilateral and contralateral hemisphere. Three days after tMCAO cell counts were highest for microglia and Ly6C^{hi} monocytes/macrophages followed by neutrophils. Lymphocytes made up a considerably smaller proportion of infiltrating cells with CD4$^+$ and CD8$^+$ T cells as equally abundant subtypes and followed by a small number of γδ T cells (Figure 2B). In the contralateral hemisphere, cell counts were on average a thousand times lower except for microglia with comparable numbers in both hemispheres (Figure 2C).

In line with comparable numbers of brain-infiltrating leukocytes, the expression levels of pro-inflammatory cytokines TNF, IL-1β, and IL-6 and the main neutrophil attracting chemokine CXCL1 in the ischemic brain measured by RT-qPCR did not vary significantly between CD73$^{-/-}$ and CD73$^{fl/fl}$ mice three days after tMCAO (Figure S3). *Tnf* showed the strongest induction by tMCAO in both CD73$^{-/-}$ and CD73$^{fl/fl}$ mice relative to the control group of sham surgery (23.84 ± 8.07-fold and 17.28 ± 1.08-fold induction, respectively),
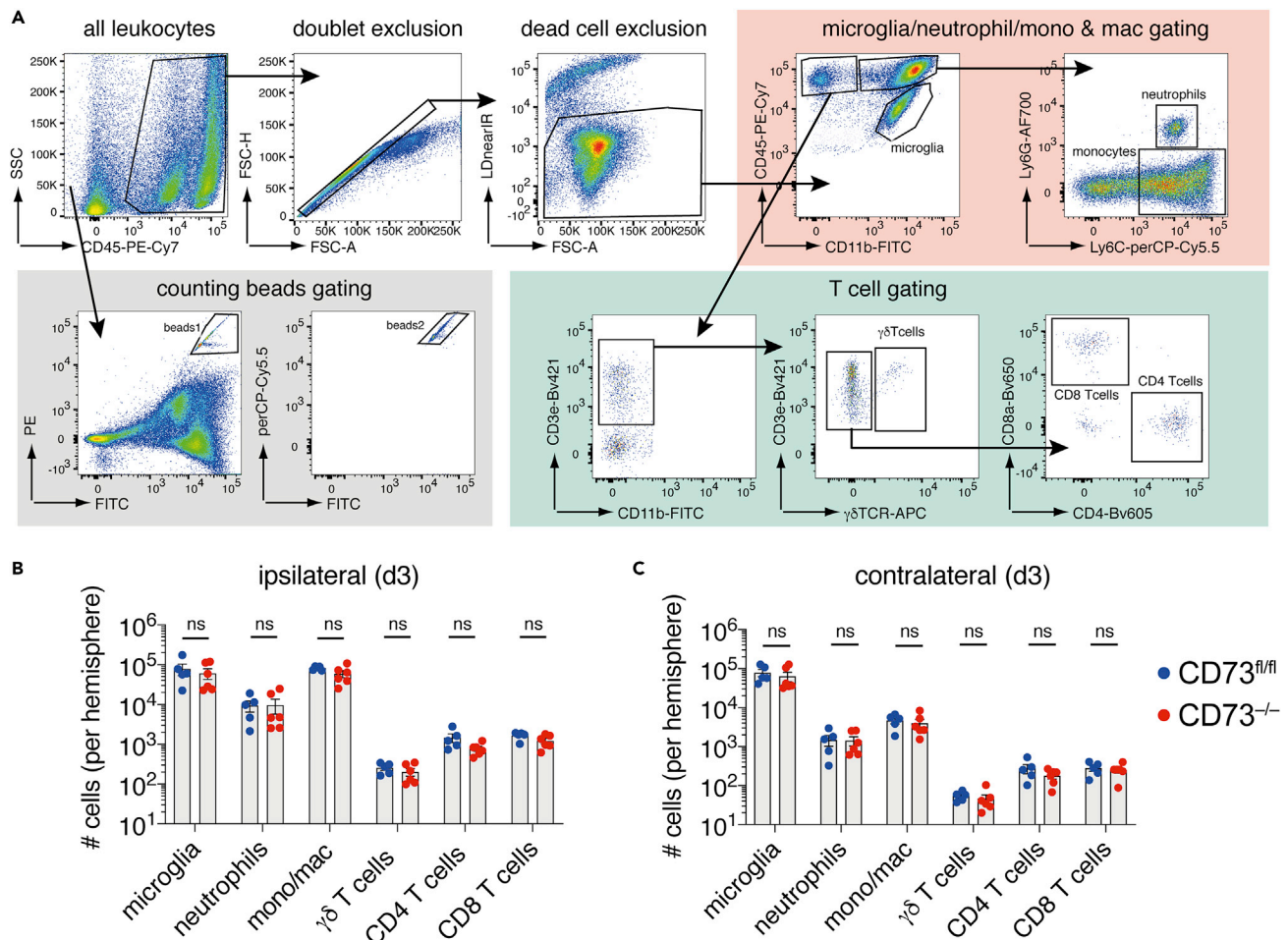
Figure 2. Leukocyte infiltration into the ischemic brain three days after tMCAO

(A) Gating strategy. Cell counts within the (B) ipsilateral and (C) contralateral hemisphere of CD73$^{-/-}$ and CD73$^{fl/fl}$ mice: microglia, neutrophils, monocytes/macrophages (mono/mac), CD4^{+}, CD8^{+}, and γδ T cells. Data are presented as mean $\pm$ SEM of three independent experiments, n = 5–6/group, unpaired two-sided Student's t test, ns = not significant.

followed by *Cxcl1* (8.77 $\pm$ 4.68-fold and 7.77 $\pm$ 3.88-fold upregulation, respectively), *Il1b* (6.06 $\pm$ 3.03-fold and 3.65 $\pm$ 1.52-fold expression, respectively), and *Il6* (3.99 $\pm$ 1.18-fold and 3.57 $\pm$ 1.43-fold induction, respectively). Taken together, CD73 deficiency did not affect *Tnf*, *Il1b*, *Il6*, and *Cxcl1* expression three days after tMCAO leading to similar numbers of infiltrating leukocytes and resident microglia.

Genetic deletion of Nt5e did not affect glial mRNA expression profile after tMCAO

To obtain a comprehensive understanding of CD73-mediated effects in ischemic stroke, we finally evaluated glial cell gene expression profiles of CD73$^{-/-}$ and CD73$^{fl/fl}$ mice three days after tMCAO with the NanoString nCounter mouse glial profiling panel. Sham surgery CD73$^{fl/fl}$ mice were used as controls.

Principal component analysis of the dataset showed a clear separation of sham and stroke data points, but CD73$^{-/-}$ and CD73$^{fl/fl}$ tMCAO samples fell in the same quadrants, indicating that the absence of CD73 does not affect the gene expression profile (Figure 3A).

In CD73$^{-/-}$ tMCAO samples, we identified 49 differentially expressed transcripts compared to sham conditions defined by a log2 fold change ≥ 1 over sham and an adjusted p value ≤ 0.05 (Figure 3B, left Volcano plot, upper right quadrant). In CD73$^{fl/fl}$ tMCAO samples, 31 genes were significantly upregulated compared to sham conditions (Figure 3B, middle Volcano plot, upper right quadrant). Differentially expressed genes included common markers of microglia activation (e.g. *Cd68*, *Tgfß1*, and *Fcrls*) or reactive

astrogliosis (e.g. *Gfap*, *Vim*, and *Serpina3n*). Moreover, many components of the complement system like *C1q*, *C4a/b*, *or C3ar1* and several chemokines (e.g. *Ccl2* and *Ccl12*) were found to be upregulated after tMCAO. Of note, we did not discover significantly downregulated genes in both genotypes after tMCAO compared to sham. Log2 fold changes of all analyzed genes with counts above threshold are supplied in a supplementary excel file online (Table S1). In line with the results of stroke size and immune cell infiltration analyses, we could not detect any differentially expressed genes between CD73$^{-/-}$ and CD73$^{fl/fl}$ tMCAO samples (Figure 3B, right Volcano plot). Accordingly, when looking at the list of differentially expressed genes after tMCAO, we saw a substantial overlap between CD73$^{-/-}$ and CD73$^{fl/fl}$ mice: All 31 significantly regulated genes in CD73$^{fl/fl}$ tMCAO samples were among the 49 differentially expressed transcripts found in CD73$^{-/-}$ tMCAO samples (Figure 3C). Of note, the additional 18 differentially expressed genes in CD73$^{-/-}$ tMCAO samples were also regulated in CD73$^{fl/fl}$ tMCAO samples compared to sham, but failed to pass either the normalized count threshold of 50 or the adjusted p value threshold of 0.05 or showed a log2 fold change just below 1.

Gene set enrichment analysis of the 49 differentially expressed transcripts in CD73$^{-/-}$ tMCAO compared to sham samples with g:Profiler demonstrated a significant enrichment of gene ontology (GO) biological process (BP) terms associated with immune response (Figure 3D). When focusing on microglia as the resident immune cells of the CNS, the gene expression profile of 50 transcripts associated with the previously described neurodegenerative phenotype (Krasemann et al., 2017) (e.g. *Cst7*, *Ctsd*, *Grn*, *Lgals3*, *Lilrb4*, *Lyz2*, *Spp1*, *Trem2*, and *Tyrobp*) clearly separated sham samples from tMCAO samples in an unsupervised hierarchical clustering analysis (Figure 3E). The same holds true for the gene expression profile of 12 selected transcripts that have previously been shown to be upregulated in astrocytes in response to ischemic stroke in an Affymetrix GeneChip mRNA analysis of eGFP-labeled astrocytes (Zamanian et al., 2012) (e.g. *Tgm1*, *Emp1*, and *Cd14*), supporting the reliability of our analysis (Figure 3F).

DISCUSSION

In the light of the strategic role of CD73 in the generation of anti-inflammatory ADO as the final step of extracellular ATP degradation, CD73 qualified as a potential immunomodulatory target in the setting of ischemic brain injury. In the present study, we demonstrated that global CD73 deficiency and acute CD73 blockade by a monoclonal antibody do not influence stroke outcome as measured by infarct volume on day three when inducing ischemia-reperfusion injury with the transient intraluminal filament model. Consistent with this finding, CD73$^{-/-}$ mice showed comparable numbers and composition of infiltrating leukocytes, comparable expression levels of pro-inflammatory cytokines and chemokines, and similar glia cell gene expression profiles on day three after stroke.

These results contrast a previous study investigating the effects of global CD73 deficiency in a different experimental stroke model, in which end arterial vessels in the middle cerebral artery territory were permanently occluded through the activation of a photosensitive dye leading to endothelial injury and subsequent platelet adhesion and thrombus formation (Petrovic-Djergovic et al., 2012). When inducing cortical infarcts with this method, CD73$^{-/-}$ mice exhibited significantly larger infarcts measured by T2-weighted magnetic resonance imaging (MRI) on day two after stroke, showed increased numbers of infiltrating leukocytes, and elevated expression levels of pro-inflammatory cytokines (Petrovic-Djergovic et al., 2012). Experiments with CD73 chimeric mice indicated that CD73 expression in the CNS rather than expression on infiltrating immune cells mediates its protective effect (Petrovic-Djergovic et al., 2012).

It seems most plausible that the conflicting findings of these experiments and our study can be attributed to the different experimental stroke models used. The main difference concerns the simultaneous development of typical cytotoxic (intracellular) edema but also pronounced vascular (extracellular) edema due to severe endothelial cell injury and thus rapid BBB breakdown induced by photothrombosis (Carmichael, 2005; Sommer, 2017). Interestingly, T2-weighted MRI imaging as applied in the aforementioned study for infarct size analysis visualizes extracellular water, i.e. vasogenic edema rather than cytotoxic edema defining the ischemic core lesion. However, vascular edema is not present to this extent in the transient intraluminal filament model applied in our study and is even absent in acute human stroke limiting the translational power of the photothrombotic model in this regard. CD73-mediated protection might be specific to photochemical endothelial cell injury and subsequent hyperacute vascular edema and could therefore not be observed in the tMCAO model characterized by ischemia-mediated BBB dysfunction and primarily cytotoxic edema.
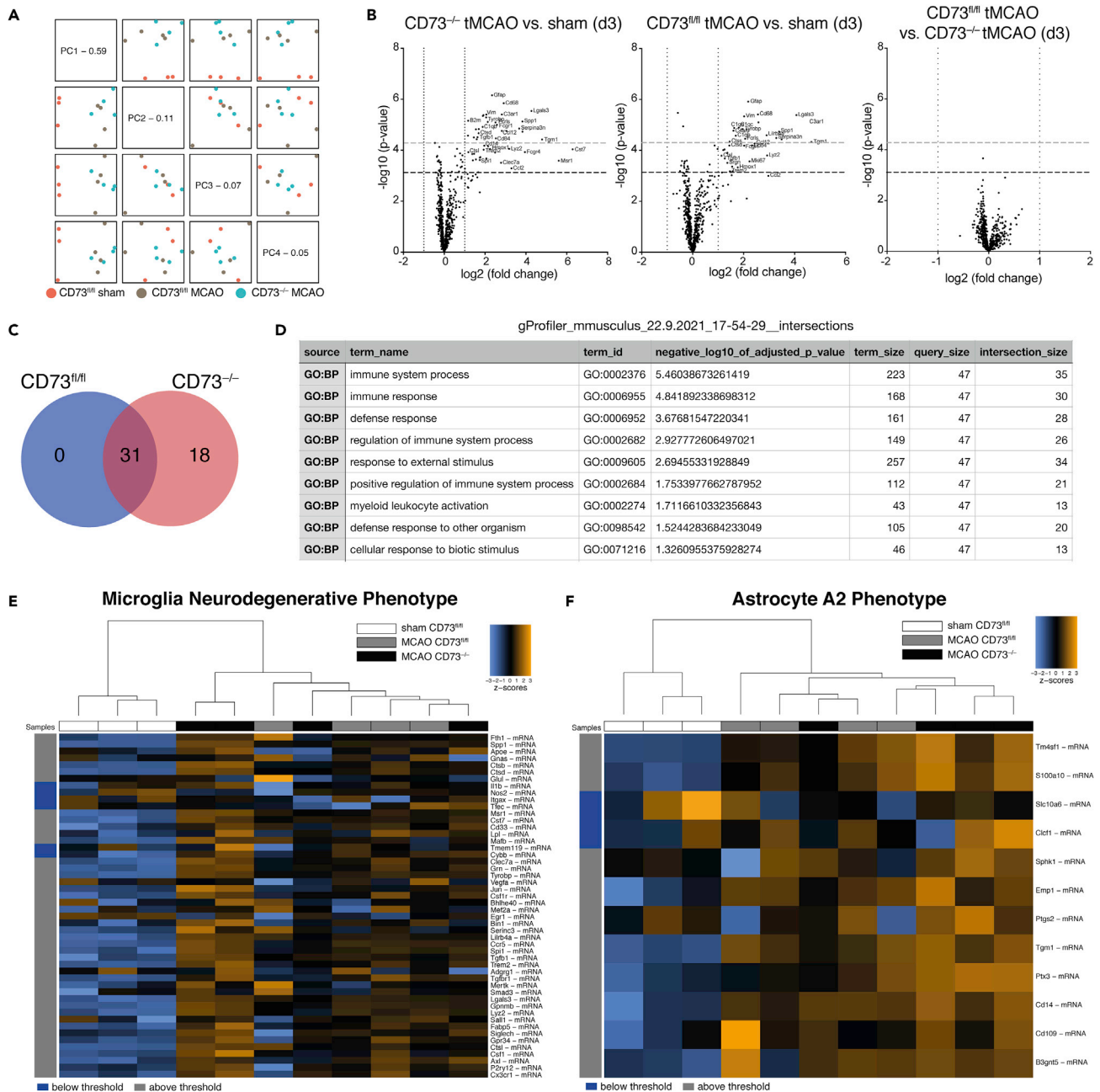
Figure 3. Glia cell gene expression profiles three days after tMCAO

(A) Principal component analysis of normalized gene expression data of CD73$^{-/-}$ tMCAO (turquoise) and CD73$^{fl/fl}$ tMCAO samples (gray) and CD73$^{fl/fl}$ sham samples (red).

(B) Volcano plots showing the fold change of genes (x axis, log2 scale) with average normalized counts >50 in CD73$^{-/-}$ and CD73$^{fl/fl}$ tMCAO samples compared to the control group of sham surgery, respectively, and compared to each other and their significance (y axis, -log10 scale). Horizontal dashed black lines indicate threshold for FDR-adjusted p values ≤ 0.05, horizontal dashed gray lines indicate threshold for FDR-adjusted p values ≤ 0.01.

(C) Venn diagram and (D) g:Profiler gene set enrichment analysis of transcripts with a log2 fold change ≥1 and an FDR adjusted p value ≤ 0.05 in CD73$^{-/-}$ (n = 49) and CD73$^{fl/fl}$ (n = 31) tMCAO samples compared to sham samples.

(E) Unsupervised hierarchical clustering and heatmap of normalized gene expression of genes associated with a microglia neurodegenerative phenotype (n = 50) in CD73$^{-/-}$ tMCAO (black) and CD73$^{fl/fl}$ tMCAO samples (gray) and CD73$^{fl/fl}$ sham samples (white).

(F) Unsupervised hierarchical clustering and heatmap of normalized gene expression of genes associated with astrocytic response to ischemia (n = 12) in CD73$^{-/-}$ tMCAO (black) and CD73$^{fl/fl}$ tMCAO samples (gray) and CD73$^{fl/fl}$ sham samples (red).

Regarding purinergic regulation of endothelial barrier function, CD73 became an interesting candidate for stroke research. Binding of ADO to A_{2A} and A_{2B} receptors on macrovascular endothelial cells leads to elevated intracellular cyclic AMP levels and improves endothelial barrier properties (Aslam et al., 2021). In line with this, CD73$^{-/-}$ mice exhibited increased vascular permeability measured by Evan's blue leakage in lung, liver, and skeletal muscle under physiological steady-state conditions, which further exacerbated during hypoxia (Thompson et al., 2004). In a comparative RNA-sequencing study on the transcriptome of murine peripheral and brain endothelial cells, *Nt5e* encoding CD73 and *Adora2a* encoding A_{2A} AR were highly expressed in the periphery (Munji et al., 2019), well explaining the dependency of peripheral endothelial barrier function on adenosine signaling. This relevance of CD73 for peripheral endothelial barrier regulation is further supported by several publications showing that CD73 mediates protection after brief and sustained periods of ischemia and reperfusion in peripheral organs like heart (Eckle et al., 2007), liver (Hart et al., 2008), or kidney (Sung et al., 2017). Unlike vascular leakage in peripheral organs of CD73$^{-/-}$ mice, CD73 deficiency did not impair endothelial barrier function in the brain even under hypoxic conditions (Thompson et al., 2004). This finding can be partially attributed to a low expression of CD73 on murine brain endothelial cells which has been consistently confirmed in several studies by immunohistochemistry (Mills et al., 2008; Petrovic-Djergovic et al., 2012) and RNA sequencing (Zhang et al., 2014; Munji et al., 2019), clearly distinguishing murine brain endothelial cells from their human and peripheral counterparts. In contrast to hypoxia-induced upregulation of CD73 on murine intestinal epithelial cells *in vivo* (Synnest-vedt et al., 2002) and human microvascular endothelial cells *in vitro* (Eltzschig et al., 2003), we did not detect an upregulation of CD73 on murine cerebral microvessels after ischemic stroke in the present study. As a further major difference between peripheral and brain endothelial cells, ADO signaling even augmented BBB permeability for intravenously injected macromolecules in mice via A_1 and A_{2A} AR activation (Carman et al., 2011).

Though barely present on brain endothelial cells at the BBB, immunohistochemistry revealed strong CD73 expression in the striatum (Augusto et al., 2013; Kulesskaya et al., 2013). In tMCAO, the striatum represents the ischemic core characterized by rapid and irreversible necrotic cell death resistant to salvage by reperfusion or neuroprotective therapeutic approaches whereas the cortex constitutes the penumbra of functionally impaired tissue predisposed for infarction but not yet irreversibly injured and thus potentially salvageable (Carmichael, 2005). Delayed neuronal cell death occurs here due to secondary mechanisms of tissue damage such as inflammation (Ramos-Cabrer et al., 2011). Since inflammation is not the primarily underlying mechanism of cell death in the striatum, CD73 can probably not confer ischemic protection by generation of anti-inflammatory ADO though highly expressed in this brain region.

Taken together, spatial distribution and comparatively low overall expression of CD73 in the murine brain and especially at the BBB likely account for the missing protective effect of this enzyme in experimental stroke induced with the tMCAO model. Compensatory ADO production in CD73$^{-/-}$ mice by other enzymes than CD73 could represent an alternative explanation for the comparable outcome of CD73$^{-/-}$ and CD73$^{fl/fl}$ mice after tMCAO as Zhang et al. demonstrated that tissue nonspecific alkaline phosphatase (TNAP) generates ADO from AMP in the brain of CD73$^{-/-}$mice (Zhang et al., 2012). However, complete compensation of CD73 deficiency by TNAP is in conflict with worse outcome of CD73$^{-/-}$mice after phto-thrombotic stroke.

In the present study, immune cell recruitment to the ischemic brain was not affected by CD73 deficiency with CD73$^{-/-}$ and CD73$^{fl/fl}$ mice exhibiting equal numbers and composition of resident microglia and infiltrating leukocytes three days after tMCAO. In the context of leukocyte infiltration, it is important to note that in experimental autoimmune encephalomyelitis (EAE) CD73 expression was required either on T cells or brain-resident cells for efficient entry of lymphocytes to the CNS (Mills et al., 2008). In EAE, ADO signaling via A_{2A} receptors at the choroid plexus (ChP), the interface between blood and cerebrospinal fluid, played a crucial role, leading to upregulation of lymphocyte adhesion molecules and paving the way for lymphocyte invasion via the ChP (Mills et al., 2008). In stroke, transendothelial migration of leukocytes across the impaired BBB was for a long time considered the main invasion route for immune cells to the ischemic brain (Benakis et al., 2018). More recent work identified the ChP of the ipsilateral lateral ventricle as predominant cerebral invasion route for T cells after cortical infarction (Llovera et al., 2017). In contrast to T cells, regional distribution of myeloid cells surrounding the ischemic core (Llovera et al., 2017) and the early detection of neutrophils in the leptomeninges and the cortical perivascular space before they invade the brain parenchyma (Perez-de-Puig et al., 2015) clearly indicate different migratory

pathways. Given that neutrophils and monocytes/macrophages are the most abundant cell populations in the ischemic hemisphere three days after stroke (Gelderblom et al., 2009), the ChP invasion route does not seem to represent the overall main migratory pathway in stroke compared to T cell-driven EAE induction. Of note, tMCAO even induces ipsilateral choroidal cell death due to transient occlusion of the supplying anterior choroidal artery (Llovera et al., 2017) further explaining equal T cell counts between CD73$^{-/-}$ and CD73$^{fl/fl}$ mice. In general, cell counts and composition of infiltrating immune cells detected in CD73$^{-/-}$ and CD73$^{fl/fl}$ mice matched well with a previous publication from our laboratory (Gelderblom et al., 2009), again underscoring that CD73-deficient mice behave like wild-type mice in this experimental stroke model.

Using NanoString technology, we demonstrated that CD73$^{-/-}$ and CD73$^{fl/fl}$ mice do not differ regarding glia cell gene expression profiles when analyzing whole brain mRNA three days after ischemic stroke. Notwithstanding, we provide data on differentially expressed transcripts between tMCAO and control (sham) samples. Significant enrichment of GO terms related to immune response among these differentially expressed genes further supports the notion of sterile inflammation as a driver of neuronal damage after ischemic stroke. In accordance with a study of Llovera and colleagues (Llovera et al., 2017), we confirmed *Ccl2* and *Ccl12* as strongly induced cytokines after tMCAO. Of note, most of the highly regulated genes associate with microglia activation in general and a neurodegenerative microglia phenotype (MGnD) in particular. This term was first coined by Krasemann and colleagues in 2017 and defines a distinct transcriptional and functional signature associated with various mouse models of neurodegeneration and characterized by a downregulation of homeostatic microglia genes like *P2ry12* or *Cx3cr1* and an upregulation of transcripts involved in lipid metabolism and phagocytosis like *Apoe* or *Cst7* (Krasemann et al., 2017). It is now proposed that the transformation of homeostatic to MGnD is a fundamental principle across various CNS pathologies in which microglia recognize neurodegeneration-associated molecular patterns (NAMPs) such as apoptotic bodies of dying neurons, myelin debris, lipid degradation products, or extracellular protein aggregates irrespective of the disease etiology (Deczkowska et al., 2018). Though limited by the resolution of bulk material analysis without cell-type-specific allocation of regulated transcripts or resolution of microglial heterogeneity, our results clearly indicate that this emerging concept also applies, at least in part, for microglial gene expression profiles in response to ischemia. Consistent with this notion, a recently published study on thalamic degeneration after cortical stroke identified this signature in a subset of microglia isolated from the degenerative thalamus 28 days after stroke (Cao et al., 2021). However, our data suggest that upregulation of transcripts associated with MGnD already occurs acutely post stroke and especially involves those genes associated with phagocytosis like *Trem2*, *Ctsd*, and *Ctsl* and pattern recognition like *Trem2*, *Lgals3*, and *Clec7a*. The crucial role of microglia phagocytotic capacity is further underlined by studies showing that Trem2$^{-/-}$ mice exhibited larger infarcts after experimental stroke (Kawabori et al., 2015; Kurisu et al., 2019). In contrast to the MGnD signature, *Tgfb1* was upregulated in tMCAO samples in our dataset suggesting some injury-specific features of microglia which were shown to be the predominant source of elevated TGF-β levels together with macrophages after stroke (Doyle et al., 2010).

In conclusion, our study demonstrated that global CD73 deficiency does not affect infarct volume, immune cell invasion, and glia cell activation profiles in a transient filament model of murine ischemic stroke. However, mRNA expression data of CD73$^{-/-}$ and CD73$^{fl/fl}$ tMCAO samples compared to sham acquired with the NanoString nCounter mouse glial profiling panel provided evidence of a microglia signature similar to the recently described neurodegenerative phenotype indicative of common molecular pathways shared between ischemic stroke and neurodegenerative diseases.

Limitations of the study

In the present study, we subjected young male mice to tMCAO and demonstrated that genetic CD73 deficiency does not affect infarct volume and leukocyte infiltration into the ischemic brain three days after stroke. Given that sex and aging influence stroke outcome and modulate the immunological response to ischemic stroke (Manwani et al., 2013; Ritzel et al., 2018), the exclusive use of young male mice is a limitation of the present study. Moreover, our findings are limited to the acute phase after stroke up to three days and further studies are required to investigate any potential role of CD73 in the context of long-term regeneration after ischemic stroke.

We validated our main finding on comparable infarct volumes by acute blockade of CD73 with a monoclonal antibody in C57BL/6J wild-type mice. Therapeutic targets in cells beyond the BBB are often

difficult to reach by monoclonal antibodies, as these usually do not cross the BBB under physiological conditions due to their high molecular weight and Fc-receptor-mediated efflux to the blood hampers efficient delivery to the brain parenchyma (Pardridge, 2012). However, after ischemic stroke, extravasation of FITC-albumin indicating BBB damage could be detected as early as 2 h after the induction of stroke (Krueger et al., 2019). As we injected the antibody twice, right before and 24 h after the induction of ischemic stroke, and rat IgG2a antibodies were shown to have a serum half-life of several days in mice (Medesan et al., 1998), we assume sufficient targeting of the brain. Alternatively, small molecule inhibitors for the acute blockade of CD73 in stroke could be used (Bhattarai et al., 2019; Lawson et al., 2020). However, they often show reduced target specificity compared with monoclonal antibodies (Imai and Takaoka, 2006).

STAR★METHODS

Detailed methods are provided in the online version of this paper and include the following:

- KEY RESOURCES TABLE
- RESOURCE AVAILABILITY
  - Lead contact
  - Materials availability
  - Data and code availability
- EXPERIMENTAL MODEL AND SUBJECT DETAILS
  - Animal experiments
- METHOD DETAILS
  - Transient middle cerebral artery occlusion model
  - Quantification of infarct volume
  - Flow cytometry of peritoneal macrophages
  - Flow cytometry of brain infiltrating leukocytes and brain resident cells
  - FACS sorting of microglia
  - Isolation of cortical microvessels
  - RNA isolation and real time quantitative PCR
  - NanoString analysis
- QUANTIFICATION AND STATISTICAL ANALYSIS

SUPPLEMENTAL INFORMATION

Supplemental information can be found online at https://doi.org/10.1016/j.isci.2022.104470.

AUTHOR CONTRIBUTIONS

ISS, OS, LP, and BR performed the experiments. JS provided essential material. ET and TM supervised the experiments and assisted with data interpretation and manuscript preparation. ISS and BR assembled the figures and wrote the manuscript, which has been reviewed by all authors.

DECLARATION OF INTERESTS

All authors declare that the research was conducted in the absence of any commercial or financial relationships that could be construed as a potential conflict of interest.

REFERENCES

Anrather, J., and Iadecola, C. (2016). Inflammation and stroke: an overview. Neurotherapeutics. 13, 661–670. https://doi.org/10.1007/s13311-016-0483-x.

Antonioli, L., Pacher, P., Vizi, E.S., and Haskó, G. (2013). CD39 and CD73 in immunity and inflammation. Trends Mol. Med. 19, 355–367. https://doi.org/10.1016/j.molmed.2013.03.005.

Aslam, M., Gündüz, D., Troidl, C., Heger, J., Hamm, C.W., and Schulz, R. (2021). Purinergic regulation of endothelial barrier function. Int. J. Mol. Sci. 22, 1207. https://doi.org/10.3390/ijms22031207.

Augusto, E., Matos, M., Sévigny, J., El-Tayeb, A., Bynoe, M.S., Müller, C.E., Cunha, R.A., and Chen, J.F. (2013). Ecto-5′- nucleotidase (CD73)-mediated formation of adenosine is critical for the striatal adenosine A2A receptor functions. J. Neurosci. 33, 11390–11399. https://doi.org/10.1523/JNEUROSCI.5817-12.2013.

Badimon, A., Strasburger, H.J., Ayata, P., Chen, X., Nair, A., Ikegami, A., Hwang, P., Chan, A.T., Graves, S.M., Uweru, J.O., et al. (2020). Negative feedback control of neuronal activity by microglia. Nature 586, 417–423. https://doi.org/10.1038/s41586-020-2777-8.

Benakis, C., Llovera, G., and Liesz, A. (2018). The meningeal and choroidal infiltration routes for leukocytes in stroke. Ther. Adv. Neurol. Dis. 11. 1756286418783708–13. https://doi.org/10.1177/1756286418783708.

Bhattarai, S., Pippel, J., Meyer, A., Freundlieb, M., Schmies, C., Abdelrahman, A., Fiene, A., Lee, S., Zimmermann, H., El-Tayeb, A., et al. (2019). X-ray Co-crystal structure guides the way to subnanomolar competitive ecto-5′-nucleotidase (CD73) inhibitors for cancer immunotherapy. Adv. Ther. 2, 1900075. https://doi.org/10.1002/adtp.201900075.

Blundon, J.A., Roy, N.C., Teubner, B.J.W., Yu, J., Eom, T.Y., Sample, K.J., Pani, A., Smeyne, R.J., Han, S.B., Kerekes, R.A., et al. (2017). Restoring auditory cortex plasticity in adult mice by restricting thalamic adenosine signaling. Science 356, 1352–1356. https://doi.org/10.1126/science.aaf4612.

Burnstock, G. (2016). An introduction to the roles of purinergic signalling in neurodegeneration, neuroprotection and neuroregeneration. Neuropharmacology 104, 4–17. https://doi.org/10.1016/j.neuropharm.2015.05.031.

Cao, Z., Harvey, S.S., Chiang, T., Foltz, A.G., Lee, A.G., Cheng, M.Y., and Steinberg, G.K. (2021). Unique subtype of microglia in degenerative thalamus after cortical stroke. Stroke 52, 687–698. https://doi.org/10.1161/STROKEAHA.120.032402.

Carman, A.J., Mills, J.H., Krenz, A., Kim, D.G., and Bynoe, M.S. (2011). Adenosine receptor signaling modulates permeability of the blood-brain barrier. J. Neurosci. 31, 13272–13280. https://doi.org/10.1523/JNEUROSCI.3337-11.2011.

Carmichael, S.T. (2005). Rodent models of focal stroke: size, mechanism, and purpose. NeuroRx 2, 396–409. https://doi.org/10.1602/neurorx.2.3.396.

Colgan, S.P., Eltzschig, H.K., Eckle, T., and Thompson, L.F. (2006). Physiological roles for ecto-5′-nucleotidase (CD73). Purinergic Signal. 2, 351–360. https://doi.org/10.1007/s11302-005-5302-5.

Deczkowska, A., Keren-Shaul, H., Weiner, A., Colonna, M., Schwartz, M., and Amit, I. (2018). Disease-associated microglia: a universal immune sensor of neurodegeneration. Cell 173, 1073–1081. https://doi.org/10.1016/j.cell.2018.05.003.

Doyle, K.P., Cekanaviciute, E., Mamer, L.E., and Buckwalter, M.S. (2010). TGFβ signaling in the brain increases with aging and signals to astrocytes and innate immune cells in the weeks after stroke. J. Neuroinflammation 7, 62. https://doi.org/10.1186/1742-2094-7-62.

Eckle, T., Krahn, T., Grenz, A., Köhler, D., Mittelbronn, M., Ledent, C., Jacobson, M.A., Osswald, H., Thompson, L.F., Unertl, K., and Eltzschig, H.K. (2007). Cardioprotection by ecto-5′-nucleotidase (CD73) and A2B adenosine receptors. Circulation 115, 1581–1590. https://doi.org/10.1161/CIRCULATIONAHA.106.669697.

Eltzschig, H.K., Ibla, J.C., Furuta, G.T., Leonard, M.O., Jacobson, K.A., Enjyoji, K., Robson, S.C., and Colgan, S.P. (2003). Coordinated adenine nucleotide phosphohydrolysis and nucleoside signaling in posthypoxic endothelium: role of ectonucleotidases and adenosine A 2B receptors. J. Exp. Med. 198, 783–796. https://doi.org/10.1084/jem.20030891.

Gelderblom, M., Leypoldt, F., Steinbach, K., Behrens, D., Choe, C.U., Siler, D.A., Arumugam, T.V., Orthey, E., Gerloff, C., Tolosa, E., and Magnus, T. (2009). Temporal and spatial dynamics of cerebral immune cell accumulation in stroke. Stroke 40, 1849–1857. https://doi.org/10.1161/STROKEAHA.108.534503.

Hart, M.L., Much, C., Gorzolla, I.C., Schittenhelm, J., Kloor, D., Stahl, G.L., and Eltzschig, H.K. (2008). Extracellular adenosine production by ecto-5′-nucleotidase protects during murine hepatic ischemic preconditioning. Gastroenterology 135, 1739–1750.e3. https://doi.org/10.1053/j.gastro.2008.07.064.

Iadecola, C., Buckwalter, M.S., and Anrather, J. (2020). Immune responses to stroke: mechanisms, modulation, and therapeutic potential. J. Clin. Invest. 130, 2777–2788. https://doi.org/10.1172/JCI135530.

Imai, K., and Takaoka, A. (2006). Comparing antibody and small-molecule therapies for cancer. Nat. Rev. Cancer 6, 714–727. https://doi.org/10.1038/nrc1913.

Jacobson, K.A., and Gao, Z.G. (2006). Adenosine receptors as therapeutic targets. Nat. Rev. Drug Discov. 5, 247–264. https://doi.org/10.1038/nrd1983.

Kawabori, M., Kacimi, R., Kauppinen, T., Calosing, C., Kim, J.Y., Hsieh, C.L., Nakamura, M.C., and Yenari, M.A. (2015). Triggering receptor expressed on myeloid cells 2 (TREM2) deficiency attenuates phagocytic activities of microglia and exacerbates ischemic damage in experimental stroke. J. Neurosci. 35, 3384–3396. https://doi.org/10.1523/JNEUROSCI.2620-14.2015.

Krasemann, S., Madore, C., Cialic, R., Baufeld, C., Calcagno, N., El Fatimy, R., Beckers, L., O'Loughlin, E., Xu, Y., Fanek, Z., et al. (2017). The TREM2-APOE pathway drives the transcriptional phenotype of dysfunctional microglia in neurodegenerative diseases. Immunity 47, 566–581.e9. https://doi.org/10.1016/j.immuni.2017.08.008.

Krishnamurthi, R.V., Ikeda, T., and Feigin, V.L. (2020). Global, regional and country-specific burden of ischaemic stroke, intracerebral haemorrhage and subarachnoid haemorrhage: a systematic analysis of the global burden of disease study 2017: A Systematic Analysis of the Global Burden of Disease Study 2017. Neuroepidemiology 54, 171–179. https://doi.org/10.1159/000506396.

Krueger, M., Mages, B., Hobusch, C., and Michalski, D. (2019). Endothelial edema precedes blood-brain barrier breakdown in early time points after experimental focal cerebral ischemia. Acta Neuropathol. Commun. 7, 17. https://doi.org/10.1186/s40478-019-0671-0.

Kulesskaya, N., Võikar, V., Peltola, M., Yegutkin, G.G., Salmi, M., Jalkanen, S., and Rauvala, H. (2013). CD73 is a major regulator of adenosinergic signalling in mouse brain. PLoS One 8, e66896. https://doi.org/10.1371/journal.pone.0066896.

Kurisu, K., Zheng, Z., Kim, J.Y., Shi, J., Kanoke, A., Liu, J., Hsieh, C.L., and Yenari, M.A. (2019). Triggering receptor expressed on myeloid cells-2 expression in the brain is required for maximal phagocytic activity and improved neurological outcomes following experimental stroke. J. Cerebr. Blood Flow Metabol. 39, 1906–1918. https://doi.org/10.1177/0271678X18817282.

Lawson, K.V., Kalisiak, J., Lindsey, E.A., Newcomb, E.T., Leleti, M.R., Debien, L., Rosen, B.R., Miles, D.H., Sharif, E.U., Jeffrey, J.L., et al. (2020). Discovery of AB680: a potent and selective inhibitor of CD73. J.Med. Chem. 63, 11448–11468. https://doi.org/10.1021/acs.jmedchem.0c00525.

Lee, Y.K., Uchida, H., Smith, H., Ito, A., and Sanchez, T. (2019). The isolation and molecular characterization of cerebral microvessels. Nat. Protoc. 14, 3059–3081. https://doi.org/10.1038/s41596-019-0212-0.

Llovera, G., Benakis, C., Enzmann, G., Cai, R., Arzberger, T., Ghasemigharagoz, A., Mao, X., Malik, R., Lazarevic, I., Liebscher, S., et al. (2017). The choroid plexus is a key cerebral invasion route for T cells after stroke. Acta Neuropathol. 134, 851–868. https://doi.org/10.1007/s00401-017-1758-y.

Manwani, B., Liu, F., Scranton, V., Hammond, M.D., Sansing, L.H., and McCullough, L.D. (2013). Differential effects of aging and sex on stroke induced inflammation across the lifespan. Exp. Neurol. 249, 120–131. https://doi.org/10.1016/j.expneurol.2013.08.011.

Medesan, C., Cianga, P., Mummert, M., Stanescu, D., Ghetie, V., and Ward, E.S. (1998). Comparative studies of rat IgG to further delineate the Fc:FcRn interaction site. Eur. J. Immunol. 28, 2092–2100.

https://doi.org/10.1002/(SICI)1521-4141(199807)28:07<2092::AID-IMMU2092>3.0.CO;2-E.

Meng, F., Guo, Z., Hu, Y., Mai, W., Zhang, Z., Zhang, B., Ge, Q., Lou, H., Guo, F., Chen, J., et al. (2019). CD73-derived adenosine controls inflammation and neurodegeneration by modulating dopamine signalling. Brain *142*, 700–718. https://doi.org/10.1093/brain/awy351.

Mills, J.H., Thompson, L.F., Mueller, C., Waickman, A.T., Jalkanen, S., Niemela, J., Airas, L., and Bynoe, M.S. (2008). CD73 is required for efficient entry of lymphocytes into the central nervous system during experimental autoimmune encephalomyelitis. Proc. Natl. Acad. Sci. U S A *105*, 9325–9330. https://doi.org/10.1073/pnas.0711175105.

Munji, R.N., Soung, A.L., Weiner, G.A., Sohet, F., Semple, B.D., Trivedi, A., Gimlin, K., Kotoda, M., Korai, M., Aydin, S., et al. (2019). Profiling the mouse brain endothelial transcriptome in health and disease models reveals a core blood–brain barrier dysfunction module. Nat. Neurosci. *22*, 1892–1902. https://doi.org/10.1038/s41593-019-0497-x.

Muzzi, M., Blasi, F., Masi, A., Coppi, E., Traini, C., Felici, R., Pittelli, M., Cavone, L., Pugliese, A.M., Moroni, F., and Chiarugi, A. (2013). Neurological basis of AMP-dependent thermoregulation and its relevance to central and peripheral hyperthermia. J. Cerebr. Blood Flow Metabol. *33*, 183–190. https://doi.org/10.1038/jcbfm.2012.157.

Niemelä, J., Ifergan, I., Yegutkin, G.G., Jalkanen, S., Prat, A., and Airas, L. (2008). IFN-β regulates CD73 and adenosine expression at the blood-brain barrier. Eur. J. Immunol. *38*, 2718–2726. https://doi.org/10.1002/eji.200838437.

Ohta, A., and Sitkovsky, M. (2001). Role of G-protein-coupled adenosine receptors in downregulation of inflammation and protection from tissue damage. Nature *414*, 916–920. https://doi.org/10.1038/414916a.

Ohta, A., Ohta, A., Madasu, M., Kini, R., Subramanian, M., Goel, N., and Sitkovsky, M. (2009). A2A adenosine receptor may allow expansion of T cells lacking effector functions in extracellular adenosine-rich microenvironments. J. Immunol. *183*, 5487–5493. https://doi.org/10.4049/jimmunol.0901247.

Pardridge, W.M. (2012). Drug transport across the blood-brain barrier. J. Cerebr. Blood Flow Metabol. *32*, 1959–1972. https://doi.org/10.1038/jcbfm.2012.126.

Perez-de-Puig, I., Miró-Mur, F., Ferrer-Ferrer, M., Gelpi, E., Pedragosa, J., Justicia, C., Urra, X., Chamorro, A., and Planas, A.M. (2015). Neutrophil recruitment to the brain in mouse and human ischemic stroke. Acta Neuropathol. *129*, 239–257. https://doi.org/10.1007/s00401-014-1381-0.

Petrovic-Djergovic, D., Hyman, M.C., Ray, J.J., Bouis, D., Visovatti, S.H., Hayasaki, T., and Pinsky, D.J. (2012). Tissue-resident ecto-5′ nucleotidase (CD73) regulates leukocyte trafficking in the ischemic brain. J. Immunol. *188*, 2387–2398. https://doi.org/10.4049/jimmunol.1003671.

Petrovic-Djergovic, D., Goonewardena, S.N., and Pinsky, D.J. (2016). Inflammatory disequilibrium in stroke. Circ. Res. *119*, 142–158. https://doi.org/10.1161/CIRCRESAHA.116.308022.

Planas, A.M. (2018). Role of immune cells migrating to the ischemic brain. Stroke *49*, 2261–2267. https://doi.org/10.1161/STROKEAHA.118.021474.

Ramos-Cabrer, P., Campos, F., Sobrino, T., and Castillo, J. (2011). Targeting the ischemic penumbra. Stroke *42* (SUPPL. 1), 7–11. https://doi.org/10.1161/STROKEAHA.110.596684.

Raudvere, U., Kolberg, L., Kuzmin, I., Arak, T., Adler, P., Peterson, H., and Vilo, J. (2019). G:Profiler: a web server for functional enrichment analysis and conversions of gene lists (2019 update). Nucleic Acids Res. *47*, W191–W198. https://doi.org/10.1093/nar/gkz369.

Reglodi, D., Tamás, A., Somogyvári-vigh, A., Szántó, Z., Kertes, E., Lenard, L., Arimura, A., and Lengvari, I. (2002). Effects of pretreatment with PACAP on the infarct size and functional outcome in rat permanent focal cerebral ischemia. Peptides *23*, 2227–2234. https://doi.org/10.1016/s0196-9781(02)00262-0.

Ritzel, R.M., Lai, Y.J., Crapser, J.D., Patel, A.R., Schrecengost, A., Grenier, J.M., Mancini, N.S., Patrizz, A., Jellison, E.R., Morales-Scheihing, D., et al. (2018). Aging alters the immunological response to ischemic stroke. Acta Neuropathol. *136*, 89–110. https://doi.org/10.1007/s00401-018-1859-2.

Schindelin, J., Arganda-Carreras, I., Frise, E., Kaynig, V., Longair, M., Pietzsch, T., Preibisch, S., Rueden, C., Saalfeld, S., Schmid, B., et al. (2012). Fiji: an open-source platform for biological-image analysis. Nat. Methods *9*, 676–682. https://doi.org/10.1038/nmeth.2019.

Schwenk, F., Baron, U., and Rajewsky, K. (1995). A cre-transgenic mouse strain for the ubiquitous deletion of loxP-flanked gene segments including deletion in germ cells. Nucleic Acids Res. *23*, 5080–5081. https://doi.org/10.1093/nar/23.24.5080.

Sommer, C.J. (2017). Ischemic stroke: experimental models and reality. Acta Neuropathol. *133*, 245–261. https://doi.org/10.1007/s00401-017-1667-0.

Sung, S.S.J., Li, L., Huang, L., Lawler, J., Ye, H., Rosin, D.L., Vincent, I.S., Le, T.H., Yu, J., Gorldt, N., et al. (2017). Proximal tubule CD73 Is Critical in renal ischemia-reperfusion injury protection. J. Am. Soc. Nephrol. *28*, 888–902. https://doi.org/10.1681/ASN.2016020229.

Synnestvedt, K., Furuta, G.T., Comerford, K.M., Louis, N., Karhausen, J., Eltzschig, H.K., Hansen, K.R., Thompson, L.F., and Colgan, S.P. (2002). Ecto-5′-nucleotidase (CD73) regulation by hypoxia-inducible factor-1 mediates permeability changes in intestinal epithelia. J. Clin. Invest. *110*, 993–1002. https://doi.org/10.1172/JCI0215337.

Thompson, L.F., Eltzschig, H.K., Ibla, J.C., Van De Wiele, C.J., Resta, R., Morote-Garcia, J.C., and Colgan, S.P. (2004). Crucial role for ecto-5′-nucleotidase (CD73) in vascular leakage during hypoxia. J. Exp. Med. *200*, 1395–1405. https://doi.org/10.1084/jem.20040915.

Zamanian, J.L., Xu, L., Foo, L.C., Nouri, N., Zhou, L., Giffard, R.G., and Barres, B.A. (2012). Genomic analysis of reactive astrogliosis. J. Neurosci. *32*, 6391–6410. https://doi.org/10.1523/JNEUROSCI.6221-11.2012.

Zhang, D., Xiong, W., Chu, S., Sun, C., Albensi, B.C., and Parkinson, F.E. (2012). Inhibition of hippocampal synaptic activity by ATP, hypoxia or oxygen-glucose deprivation does not require CD73. PLoS One *7*, e39772. https://doi.org/10.1371/journal.pone.0039772.

Zhang, Y., Chen, K., Sloan, S.A., Bennett, M.L., Scholze, A.R., O'Keeffe, S., Phatnani, H.P., Guarnieri, P., Caneda, C., Ruderisch, N., et al. (2014). An RNA-sequencing transcriptome and splicing database of glia, neurons, and vascular cells of the cerebral cortex. J. Neurosci. *34*, 11929–11947. https://doi.org/10.1523/JNEUROSCI.1860-14.2014.

STAR★METHODS

KEY RESOURCES TABLE

REAGENT or RESOURCE	SOURCE	IDENTIFIER
Antibodies		
Anti-mouse CD73 (TY/23)	Bio X Cell	Cat# BE0209; RRID:AB_10950310
Rat IgG2a isotype control (2A3)	Bio X Cell	Cat# BP0089; RRID:AB_1107769
Anti-mouse CD3e (BV421; 17A2)	Biolegend	Cat# 100228; RRID:AB_2562553
Anti-mouse CD4 (BV605; RM4-5)	Biolegend	Cat# 100548; RRID:AB_2563054
Anti-mouse CD8a (BV650; 53–6.7)	Biolegend	Cat# 100742; RRID:AB_2563056
Anti-mouse CD11b (FITC; M 1/70)	Biolegend	Cat# 101206; RRID:AB_312789
Anti-mouse CD11b (PE-CF594; M 1/70)	BD Horizon	Cat# 562287; RRID:AB_11154216
Anti-mouse CD45 (PE-Cy7; 30-F11)	Biolegend	Cat# 103114; RRID:AB_312979
Anti-mouse CD45 (PerCP; 30-F11)	Biolegend	Cat# 103130; RRID:AB_893339
Anti-mouse CD45 (APC-eF780; 30-F11)	eBioscience/Thermo Fisher Scientific	Cat# 47-0451-82; RRID:AB_1548781
Anti-mouse CD73 (BV421; TY/11.8)	Biolegend	Cat# 127217; RRID:AB_2687251
Anti-mouse FceR1 (PE; MAR-1)	Biolegend	Cat# 134307; RRID:AB_1626104
Anti-mouse γδ T cell receptor (APC; eBioGL3)	eBioscience/Thermo Fisher Scientific	Cat# 17-5711-82; RRID:AB_842756
Anti-mouse Ly6C (PerCP-Cy5.5; HK1.4)	Biolegend	Cat# 128012; RRID:AB_1659241
Anti-mouse Ly6G (AF700; 1A8)	Biolegend	Cat# 127622; RRID:AB_10643269
Anti-mouse O4 (PE; O4)	Miltenyi Biotec	Cat# 130-117-507; RRID:AB_2733886
Chemicals, peptides, and recombinant proteins		
Bovine serum albumin (BSA)	Sigma-Aldrich	Cat# A7906-500G
Collagenase A	Roche	Cat# 11088793001
Chloroform	Sigma-Aldrich	Cat# 288306-100ML
Dextran ultrapure MW 60.000–90.000	Thermo Fisher Scientific	CAS 9004-54-0
D-Mannitol ≥ 98%	Sigma-Aldrich	Cat# M4125-500G
DMEM 1x medium	Gibco	Cat# 41965-039
DNase I	Roche	Cat# 11284932001
Ethylenediaminetetraacetic acid (EDTA)	Sigma-Aldrich	Cat# 03690-100ML
MCDB 131 medium	Gibco	Cat# 0372019
Papain 24 U/ml	Worthington	Cat# LK003176
Percoll™ PLUS	Cytiva	Cat# 17544501
Phosphate-buffered saline (PBS)	Sigma-Aldrich	Cat# D8537-1L
2,3,5-Triphenyl-2-hydroxy-tetrazolium chloride (TTC)	Sigma-Aldrich	Cat# T887-100G
Tris-EDTA buffer solution	Sigma-Aldrich	Cat# 93283-100ML
TRIzol	Ambion	Cat# 15596026
Critical commercial assays		
LIVE/DEAD™ Fixable Near-IR Dead Cell Stain Kit	Invitrogen	Cat# L10119
Maxima First Strand cDNA Synthesis Kit for qRT-PCR	Thermo Fisher Scientific	Cat# K1642
Maxima Probe qPCR Master Mix (2X)	Thermo Fisher Scientific	Cat# K0262
RNeasy Micro Kit	Qiagen	Cat# 74004
RNeasy Mini Kit	Qiagen	Cat# 74106
nCounter Mouse Glial Profiling Panel	Nanostring	XT-CSO-M Glial Profiling-12

Continued

REAGENT or RESOURCE	SOURCE	IDENTIFIER
Deposited data		
NanoString data	Nanostring Core Facility	GSE203161
Experimental models: Organisms/strains		
CD73^fl/fl (Nt5e^tm2Jsc)	University Medical Center Hamburg-Eppendorf	MGI ID: 6257868
Tg(CMV-cre)1Cgn	University Medical Center Hamburg-Eppendorf	MGI ID: 2176180
Tg(CMV-cre)1Cgn x CD73^fl/fl (Nt5e^tm2Jsc)	University Medical Center Hamburg-Eppendorf	N/A
C57BL/6J	Charles River Laboratories	N/A
Oligonucleotides		
Actb (Mm00607939_s1)	Thermo Fisher Scientific	Cat# 4331182
Cxcl1 (Mm04207460_m1)	Thermo Fisher Scientific	Cat# 4331182
Il1b (Mm00434228_m1)	Thermo Fisher Scientific	Cat# 4331182
Il6 (Mm00446190_m1)	Thermo Fisher Scientific	Cat# 4331182
Nt5e (Mm00501910_m1)	Thermo Fisher Scientific	Cat# 4331182
Sdha (Mm01352366_m1)	Thermo Fisher Scientific	Cat# 4331182
Tnc (Mm00495662_m1)	Thermo Fisher Scientific	Cat# 4331182
Tnf (Mm00443258_m1)	Thermo Fisher Scientific	Cat# 4331182
Software and algorithms		
Fiji ImageJ v. 2.1.0/1.53c	(Schindelin et al., 2012)	https://imagej.net/software/fiji/
FlowJo^TM v. 10.8	BD Life Sciences	
g:Profiler v. e104_eg51_p15_3922dba	(Raudvere et al., 2019)	https://biit.cs.ut.ee/gprofiler/gost
GraphPad Prism v. 9.2.0	GraphPad Software	N/A
Illustrator v. 25.2	Adobe	N/A
Microsoft Excel v. 16.58	Microsoft Corporation	N/A
nSolver Analysis Software v. 4.0	Nanostring® Technologies Inc.	N/A
Other		
tMCAO suture	Docoll	Cat# 602312PK10Re
Isoflurane	Baxter	HDG9623
Buprenorphine (Temgesic®) 0.324 mg/mL	Indivior Europe Ltd.	PZN: 00345928
Tramadol Hydrochloride (Tramal®) 100 mg/mL	Grünenthal GmbH	PZN: 11236208
BD TruCount^TM tubes	BD Biosciences	Cat# 663028

RESOURCE AVAILABILITY

Lead contact

Requests for further information or resources and reagents should be directed to the lead contact, Björn Rissiek (b.rissiek@uke.de).

Materials availability

This study did not generate new unique reagents.

Data and code availability

Data reported in this paper will be shared by the lead contact upon request. NanoString data are deposited in a publicly accessible database. NanoString data with log2 fold changes of all analyzed genes with counts above threshold are supplied in a supplementary excel file (Table S1). Nanostring raw data can be downloaded under the accession number GSE203161. This paper does not report original code. Any additional information required to reanalyze the data reported in this paper is available from the lead contact upon request.

EXPERIMENTAL MODEL AND SUBJECT DETAILS

Animal experiments

All animal experiments were approved by the local animal care committee (Behörde für Justiz und Verbraucherschutz, project number N006/2018) and conducted according to the guidelines of the animal facility of the University Medical center Hamburg-Eppendorf. Transgenic mice were backcrossed at least 10 generations to the C57BL/6 background. Mice with global deficiency in CD73 (CD73$^{-/-}$) were generated by crossing CD73$^{fl/fl}$ mice (Nt5e^{tm2Jsc}, MGI ID: 6257868) with a B6 mouse strain expressing the Cre recombinase under the control of human cytomegalovirus minimal promoter (Tg(CMV-cre)1Cgn, MGI ID: 2176180), mediating the deletion of loxP-flanked genes in all tissues including germ cells (Schwenk et al., 1995). Since Nt5e^{tm2Jsc} have a congenic background and therefore still contain genetic material of the used 129-derived embryonic stem cells we used CD73$^{fl/fl}$ as control throughout all experiments. C57BL/6J wildtype mice were purchased from Charles River. Young male mice (25-30 g, 11-16 weeks old) were used throughout all experiments.

METHOD DETAILS

Transient middle cerebral artery occlusion model

Transient middle cerebral artery occlusion (tMCAO) was achieved with the intraluminal filament method using a silicone coated nylon filament (Docoll, 602312PK10Re). Briefly, the common carotid artery was exposed via a ventral midline neck incision, the filament was introduced via the common carotid artery into the internal carotid artery and advanced until the origin of the middle cerebral artery was blocked. After 50 min of occlusion the filament was withdrawn and blood flow was restored (reperfusion). Sufficient occlusion was controlled by transcranial temporal laser Doppler (moor instruments) of the left MCA territory compared to the contralateral side. Control animals (sham) underwent the same procedure without insertion of the filament.

All mice were anesthetized with isoflurane (Baxter) at a concentration of 1.8% vol/vol oxygen and underwent analgesia with buprenorphine (Indivior Europe Ltd.) (0.03 mg/kg body weight s.c.). During surgery heart rate, respiratory rate, oxygen saturation and rectal body temperature were measured after filament insertion and removal. Every mouse was scored twice daily on a scale from 0 to 5 (0, no deficit; 1, preferential turning; 2, circling; 3, longitudinal rolling; 4, no movement; 5, death) and injected with 0.7 mL 0.9% NaCl i.p. in case of weight loss greater than 10% of initial weight. For management of postsurgical pain mice were supplied with tramadol hydrochloride (Grünenthal) via the drinking water at a concentration of 1 mg/mL.

For the acute blockade of CD73, C57BL/6J mice were injected with 100 μg of anti-mouse CD73 antibody (TY/23) or rat IgG2a isotype control antibody (2A3) i.p. in 100 μL 0.9% NaCl right before the induction of ischemic stroke and for a second time 24 h after reperfusion.

Quantification of infarct volume

For analysis of infarct size, mice were deeply anesthetized with isoflurane and killed by cercival dislocation three days after reperfusion. Brains were harvested and cut into 6 1 mm thick slices (Braintree Scientific) excluding the olfactory bulb and the cerebellum. Vital staining was performed with 2% (w/v) 2,3,5-triphenyl-2-hydroxy-tetrazolium chloride (TTC, Sigma-Aldrich) in phosphate-buffered saline (PBS, Sigma-Aldrich) with 5% (w/v) D-Mannitol (Sigma-Aldrich). Infarct volumes were determined using Fiji ImageJ version 2.1.0/1.53c (Schindelin et al., 2012). Edema correction of infarct volume was performed using the method published by Reglodi et al.: Edema-corrected stroke volume was calculated as the product of absolute unadjusted infarct area and contralateral hemisphere area divided by ipsilateral hemisphere area (Reglodi et al., 2002).

Flow cytometry of peritoneal macrophages

Mice were deeply anesthetized with isoflurane and killed by cervical dislocation. Peritoneal lavage was performed with 5 mL PBS supplemented with 1 mM ethylenediaminetetraacetic acid (EDTA, Sigma-Aldrich) and cells were washed once with FACS buffer (PBS containing 0.2% w/v bovine serum albumin (BSA, Sigma-Aldrich) and 0.5 mM EDTA). Cells were stained with surface antibodies against CD11b (FITC; M1/70), FceR1 (PE; MAR-1) and CD73 (BV421; TY/11.8) at a concentration of 1:100. Data were acquired with a BD FACSCelesta^{TM} Cell Analyzer (BD Biosciences) and analyzed with FlowJo^{TM} version 10.8 (BD Life Sciences).

Flow cytometry of brain infiltrating leukocytes and brain resident cells

Mice were deeply anesthetized with isoflurane and perfused via the left ventricle with PBS and brains were harvested. For flow cytometry of brain infiltrating leukocytes only animals with a visible cortical infarct were included for subsequent analysis and ipsilateral and contralateral hemispheres were dissected separately. Mice used for flow cytometry of brain resident cells to study CD73 expression on oligodendrocytes did not have a stroke and brains were processed as a whole. Dissected brains were digested for 30 min at 37°C (1 mg/mL collagenase A (Roche), 0.1 mg/mL DNase I (Roche) in DMEM 1x (Gibco) and passed through a 70 μm cell strainer. Cells were incubated with ACK erythrocyte lysis buffer on ice and separated from myelin and debris by Percoll™ PLUS (Cytiva) gradient centrifugation (33% with PBS). For the analysis of brain infiltrating leukocytes cells were stained for 30 min at 4°C with surface antibodies against CD11b (FITC; M 1/70), CD45 (PE-Cy7; 30-F11), γδ T cell receptor (APC; eBioGL3), Ly6G (AF700; 1A8), CD3e (BV421; 17A2), CD8a (BV650; 53–6.7), CD4 (BV605; RM4-5) and Ly6C (PerCP-Cy5.5, HK1.4) at a concentration of 1:100 and live/dead™ fixable near-IR dead cell staining (Invitrogen). For the analysis of CD73 expression on oligodendrocytes the following antibodies were used: anti-CD45 (PerCP; 30-F11) and anti-CD73 (BV421; TY11.8) at a concentration of 1:100 and anti-O4 (PE; O4) at a concentration of 1:50.

After staining, cells were washed with FACS buffer and transferred to BD TruCount™ tubes (BD Biosciences) for absolute cell quantification of infiltrating leukocytes. Data was acquired with a BD FACSCelesta™ Cell Analyzer (BD Biosciences) and analyzed by FlowJo™ version 10.8 (BD Life Sciences).

FACS sorting of microglia

One day after stroke induction, mice were deeply anesthetized with isoflurane and perfused via the left ventricle with PBS. Brains were harvested and only animals with a visible cortical infarct were included for subsequent FACS sorting. Ipsilateral and contralateral hemispheres were dissected separately, digested for 30 min at 37°C (24 U/ml Papain (Worthington) for 20 min and 1 mg/mL collagenase, 0.1 mg/mL DNAse I in DMEM for additional 10 min) and pressed through a 100 μm cell strainer. Cells were separated from myelin and debris by two phase Percoll gradient centrifugation and stained with surface antibodies (30 min, 4°C) against CD45 (APC-eF780; 30-F11) and CD11b (PE-CF594; M 1/70) at a concentration of 1:100. After doublet exclusion microglia were sorted as CD45 intermediate and CD11b positive at a BD FACSAria™ Fusion Flow Cytometer (BD Biosciences).

Isolation of cortical microvessels

Cortical microvessels were collected according to a protocol previously published by Lee et al. (2019) with a slight modification regarding Dextran centrifugation. C57BL/6J wildtype mice were deeply anesthetized with isoflurane and killed by cervical dislocation one day after tMCAO. Brains were harvested and rolled on cellulose chromatography paper to remove the meninges. Brains (excluding olfactory bulb and cerebellum) were sliced sagitally (2 mm) and cortices were isolated by removing all deep brain structures. Cortical tissue was homogenized in MCDB 131 medium (Gibco) using a tissue grinder (10 strokes in 1 mL medium, additional 2 strokes in 2 mL medium), centrifugated (2.000 g, 5 min, 4°C) and separated from myelin and debris by 15% (w/v PBS) Dextran (Thermo Fisher Scientific) density centrifugation (4.500 g, 15 min, 4°C). Microvessels were retrieved from the final red pellet with a 40 μm cell strainer in MCDB 131 medium containing 0.5% (w/v) BSA.

RNA isolation and real time quantitative PCR

RNA from sorted microglia was isolated using the RNeasy Micro Kit (Qiagen) according to the manufacturer's protocol. RNA from cortical microvessels was isolated using the RNeasy Mini Kit (Qiagen). RNA concentration and integrity were determined with the Agilent Bioanalyzer System.

To isolate RNA from brain tissue mice were sacrificed by isoflurane overdose and cervical dislocation three days after stroke induction. Only animals with a visible cortical and striatal infarct after slicing the brain into 1 mm sections were included for subsequent RNA extraction. Brains were homogenized in 1 mL TRIzol reagent per 50-100 mg tissue (Ambion) using a tissue grinder and IKA® Ultra Turrax®, chloroform (Sigma-Aldrich) was added, samples were centrifuged at 12000g for 15 min at 4°C and the upper aqueous phase was collected. RNA was precipitated by addition of isopropyl alcohol, washed with 75% ethanol and dissolved in Tris-EDTA buffer solution (Sigma-Aldrich). RNA concentration and quality (260/280 ratio) were quantified using NanoDrop 2000c spectrophotometer (peqlab). For subsequent real time quantitative

PCR (RT-qPCR) on selected cytokines and chemokines whole brain RNA was purified using the RNeasy Mini Kit (Qiagen).

Complementary DNA was transcribed using the Maxima First Strand cDNA Synthesis Kit for qRT-PCR (Thermo Fisher Scientific). RT-qPCR primers (*Actb* Mm00607939_s1, *Sdha* Mm01352366_m1, *Nt5e* Mm00501910_m1, *Tnc* Mm00495662_m1, *Il1b* Mm00434228_m1, *Il6* Mm00446190_m1, *Tnfa* Mm00443258_m1, *Cxcl1* Mm04207460_m1) and probe mixtures (Maxima Probe qPCR Master Mix) were obtained from Thermo Fisher Scientific. RT-qPCR analysis was performed on a LightCycler96 from Roche.

Relative gene expression data were obtained with the ΔCt method using an appropriate housekeeping gene (Sdha for microglia and whole brain RNA, β-Actin for microvessels) and by normalizing $2^{-\Delta Ct}$ values of the control group to 1.

NanoString analysis

The NanoString nCounter® mouse glial profiling panel was used to evaluate the expression of 770 predefined genes involved in glial cell biology in both homeostasis and disease. 50 ng of whole brain mRNA from sham surgery CD73$^{fl/fl}$ mice, stroked CD73$^{fl/fl}$ mice and stroked CD73$^{-/-}$ mice (n = 4 / group) were hybridized to the cartridge and the chip was run on a nCounter SPRINT profiler by the NanoString core facility at the the University Medical Centre Hamburg-Eppendorf. Raw count data were analyzed using the advanced analysis module for nSolver version 4.0 (NanoString® Technologies Inc.). A cutoff for background signal was introduced at 50 counts as the value of the highest negative control present on the chip plus 30 counts. All samples passed the quality controls for positive control normalization and imaging, four samples showed a binding density above the default threshold of 1.8 and led to a quality control warning, but positive control linearity was not affected. One sham sample was excluded from further analysis due to low binding density. Using the geNorm algorithm 11 out of 13 housekeeping genes were selected for normalization (*Ccdc127, Mto1, Aars, Lars, Tada2b, Fam104a, Xpnpep1, Csnk2a2, Tbp, Cnot10, Supt7l*), the normalization factor ranged between −0.2 and 0.1 with a mean squared error of reference mRNAs from mean profile between 0.02 and 0.1. Differential gene expression between each of the two experimental stroke groups and the control group (sham surgery) was calculated with an algorithm consisting of the simplified negative binomial model and the linear regression method. p-values were false discovery rate (FDR)-adjusted with the Benjamini-Yekutieli method to correct for multiple testing. For differentially expressed genes, we performed a gene set enrichment analysis with g:Profiler (version e104_eg51_p15_3922dba) (Raudvere et al., 2019). The background set was limited to the genes analyzed with the NanoString nCounter® mouse glial profiling panel (statistical domain scope: custom over annotated genes) and the default g:SCS algorithm was used to correct for multiple testing applying a significance threshold of 0.05.

QUANTIFICATION AND STATISTICAL ANALYSIS

Data are reported as mean ± standard deviation (SD) or mean ± standard error of the mean (SEM) as indicated in figure legends. Statistical analyses were performed with the appropriate test indicated in the figure legends using GraphPad Prism version 9.2.0 (GraphPad Software). Briefly, the Student's t-test was used to compare infarct volumes and immune cell counts between two groups of interest and ordinary one-way ANOVA was performed for multiple comparisons with Tukey's correction for multiple testing. p-values < 0.05 were considered statistically significant. Figures were designed with Illustrator version 25.2 (Adobe).